Mirror Images of Atmospheric Flow

H. M. VAN DEN DOOL

Cooperative Institute for Climate Studies, Department of Meteorology, University of Maryland, College Park, Maryland

(Manuscript received 24 July 1990, in final form 3 March 1991)

ABSTRACT

We address whether there are pairs of instantaneous 500-mb flow patterns that are, relative to the climatology, as much as possible each other's opposite (which we term "mirror images" or "antilogs"), and we investigate whether such flows are followed by opposite 12-h time tendencies.

Over eastern North America for almost all wintertime flow patterns in a 15-yr dataset it is almost as easy to find an antilog as an analog. Exceptions are very deep lows for which no mirror-imaged highs exist. In addition, antilogs make for 12-h height forecasts at a skill level almost as good as those based on analogs.

Therefore the multivariate height distribution (i.e., flow patterns) is almost symmetric, and mirror imaging an observed flow is likely to yield a physically plausible pattern although not necessarily observed so far. Note that time tendencies tend to be opposite for opposite initial conditions for short periods of time even though the perturbations (full anomalies) are not small. An explanation of the latter is sought by running a global barotropic model from both regular and mirror-imaged initial conditions. Out to 12 h the tendency of the midlatitude streamfunction is primarily determined by the linear part of the absolute vorticity advection. However, on small scales (i.e., the vorticity field) forecasts deteriorate after about 6 h when the nonlinear term is either omitted (linear run) or represented wrongly (in the mirror-imaged run).

1. Introduction

It has long been assumed that if two observed atmospheric states are very close initially they will remain close for some time to follow. This intuitive assumption has two aspects that need to be distinguished, one diagnostic and one prognostic. The analog diagnostic (AD) aspect is concerned with identifying atmospheric states that are so close that they can be called each others' analog. Using the development following a historical analog to forecast future atmospheric flow is the prognostic aspect called analog forecasting (AF).

A major problem with AD (and therefore AF) is that there are no good analogs to begin with (Lorenz 1969; Gutzler and Shukla 1984; Shabbar and Knox 1986; Ruosteenoja 1988; Toth 1991). This is generally attributed to the short historical record (order 10–100 yr), which makes it highly unlikely to find two matching atmospheric states given the large variety of atmospheric flow. As a result AF is not a short-range forecast procedure of any great practical value—it is outperformed even by persistence. Also the far superior competition of numerical methods already available excludes AF from practical consideration.

We have shown recently (van den Dool 1989, hereafter D89) that on a limited area (circle with radius $r < 1000$ km), it is possible to find many good analogs on instantaneous 500-mb height in a dataset of only 15 yr, several of which are to within observational error of each other. It was also shown that these analogs have a modest capability to forecast the height at the center of the circle 12 h later. In particular, limited-area AF is demonstrably better than persistence, a capability entirely missing in previous studies. This allows us to look more seriously into the 12-h changes, following initially similar conditions.

In the field of monthly and seasonal forecasting AF is still of some practical value. It was in this context that the notion antilog was invented (Harnack et al. 1985) as a means to alleviate somewhat the problem of short records. Antilogs are flow anomaly patterns that are each other's opposite; i.e., each other's mirror image relative to the climatology. In the working definition given in section 2 antilogs are constructed by changing the sign of the departures from climatology (anomalies). In this sense, anomalous highs become anomalous lows and vice versa. In AF, antilogs would be as interesting as analogs if (i) we can find good quality antilogs in the historical records (the diagnostic aspect) and (ii) if opposite patterns imply opposite subsequent time tendencies (the prognostic aspect).

Combining the experience at both short and long forecast ranges we tried, out of curiosity, AD and AF through antilogs in an experiment that was otherwise identical to that in D89. The results will be described in detail in section 2, but by way of introduction it

Corresponding author address: Dr. Huug M. van den Dool, Prediction Branch, Climate Analysis Center, W/NMC51, WWB, Room 604, Washington, DC 20233.

suffices to say that we could find antilogs almost as easily as analogs, and that 12-h height forecasts based on antilogs are nearly as skillful as those based on analogs. Even though the inclusion of antilogs short-range AF remains impractical, the behavior of analogs versus antilogs raises intriguing questions about the linearity and symmetry, or absence thereof, of atmospheric flow relative to its climatology. For example, (i) Is the mirror image of a given flow as likely to occur as the flow itself? and (ii) Why would the atmosphere have opposite time tendencies following opposite initial conditions? Although both address "nonlinearity" in a loose sense, (i) and (ii) require different answers.

Concerning (i) it has to be pointed out immediately that if heights were to have symmetric frequency distributions the existence of antilogs at a single point is a trivial matter. For asymmetric distributions good antilogs are, diagnostically, less likely than good analogs. These properties will be studied here for patterns (or a collection of grid points) rather than single grid points. While we expect the result of White (1980), who investigated skewness on a point-by-point basis, to carry over to patterns, the dynamics could place possibly different constraints on permissible flow patterns for positive and negative anomalies.

Because we suspect (D89) that AF based on analogy in terms of 500-mb height ought to work somewhat like a barotropic model, we present in section 3 the barotropic model as a dynamical paradigm for analog/antilog behavior. We have made a series of numerical 12-h forecasts using a classic barotropic model starting from regular (i.e., observed) as well as mirror-imaged initial conditions. Although this was done primarily to investigate question (ii), we use the opportunity to show that a linear barotropic model, by necessity, makes 12-h height forecasts on a skill level not much less than a regular nonlinear barotropic model. In some sense we quantify the amount of nonlinearity associated with perturbations as big as day-to-day anomalies.

The idea of using antilogs was born in the field of long-range forecasting where antecedent time-averaged conditions are often used to select analogs (or antilogs). However, the new work presented here exclusively pertains to instantaneous flow. Comparisons with long lead times and time-averaged flow will be postponed until the discussion section.

2. Analogs and antilogs: Empirical findings

a. Data, terminology, and analog searching

We briefly repeat here the analog searching procedure described in D89 (see their Fig. 1). The process is almost selfevident. The base B is the situation for which the analogs are sought. The analog A is the best match found in some year at some time. The verification and the forecast are valid 12 h after B and A, respectively. More than one analog ($A_1, A_2, \ldots$) and subsequent forecasts ($F_1, F_2, \ldots$) can be considered. The initial "error" of AF can be measured by $B - A$ while the forecast accuracy is measured by $F - V$ which should be compared to persistence $V - B$.

Analogs are sought here by calculating the rms difference between the base height field (Z^B) and the height field of a candidate analog (Z^{CA}) over all collocated 13 grid points at or within a circle of radius 900 km around the target point at 38°N, 80°W (see Fig. 2 in D89 and text). Many other measures of similarity have been tried (see also Toth 1991), but none turned out convincingly better than the simple rms difference referred to as the quality Q. The data used here consist of twice-daily 500-mb height analyses from the National Meteorological Center, Washington D.C., United States, on a 4° × 5° latitude–longitude grid from 1963 to 1977.

For a given base there are about 1800 candidate analogs. So in all, 1800 Q's have to be calculated and are ranked from low to high, the lowest Q being the best analog (A_1) etc. It should be emphasized that even though we search for analogs over a circular area, we will verify the forecast only at the target grid point. This is done to stop the propagation of large errors from the unmatched exterior into the verification area (see D89).

We checked for analogy in the 500-mb height only. The least we hoped for was that analogy in heights would guarantee the advection of vorticity to be similar. Since advection is known to be a major component of the tendencies at 500 mb (where divergence is normally relatively small) we hoped to be able to make "barotropic" AF with some degree of success.

The search for antilogs proceeds in the same fashion after the candidate is mirror imaged by

$$Z^*_{CA} = -(Z_{CA} - C) + C, \qquad (1)$$

i.e. we take out the climatology, change the sign of the anomalies, and add the climatology back. An example of an observed flow pattern and its mirror image are shown in Fig. 1. In a good-sized test it turned out that, to those individuals asked, it is not immediately obvious which of the two flows has been observed and which has been constructed. This testifies to the apparent realism of mirror-imaged maps in most cases. Using the Z^*_{CA}'s and ranking the 1800 new Q's, yields a list of antilogs for a given base case.

b. Diagnostics of analogs and antilogs

In Table 1 we show the rms qualities Q for the top 13 analogs and antilogs for the flow pattern (an arbitrarily chosen base) observed on 0000 UTC 30 January 1966. The quality of the match (i.e., 47.2 gpm) should be judged against the background of rms differences of randomly selected cases, which is 225 gpm in this area

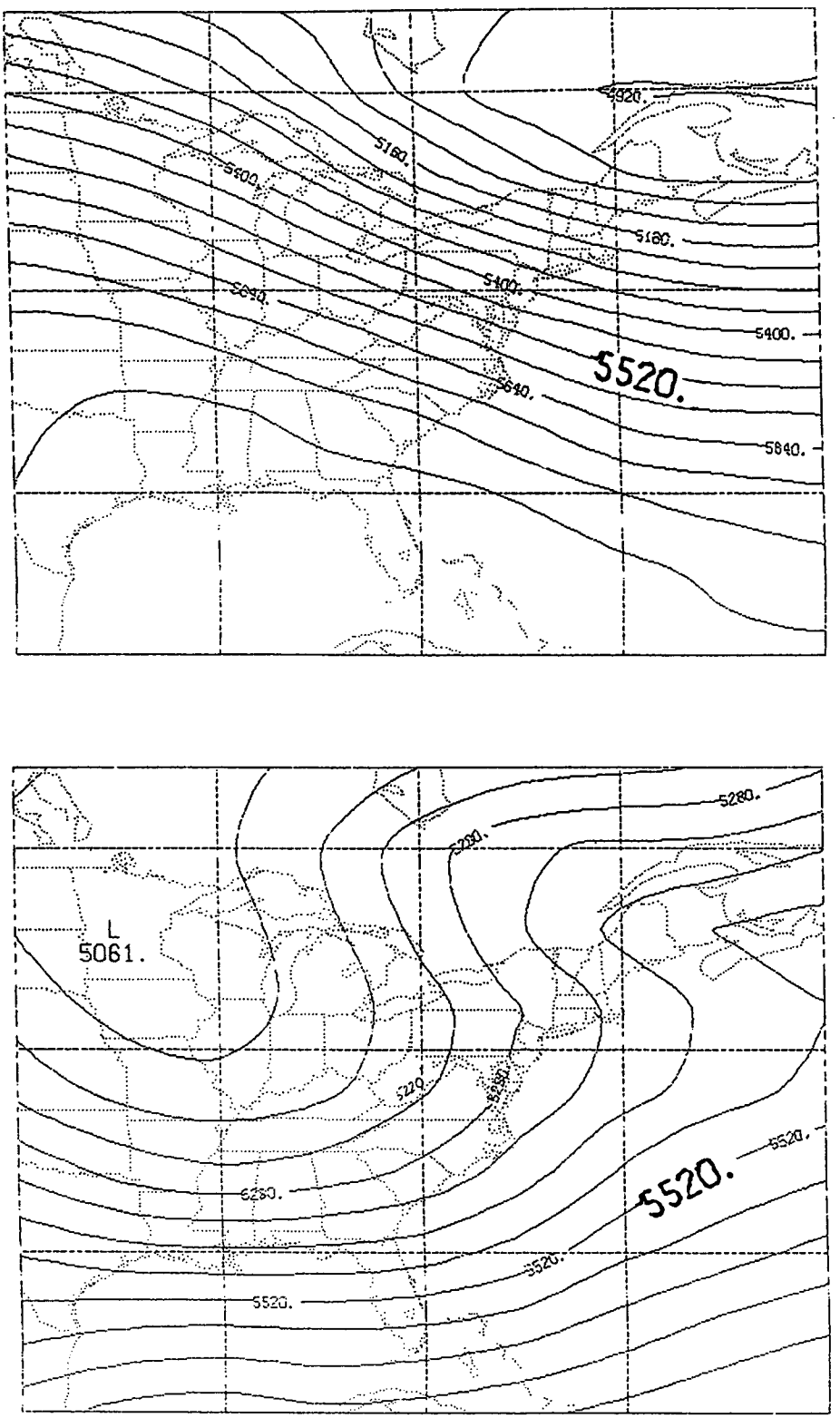

FIG. 1. A pair of flow patterns that are each other's mirror image. The upper one has been observed on 0000 UTC 17 January 1974. Its mirror image (bottom) is a close match to 0000 UTC 30 January 1966 on the 13 grid points surrounding 38°N, 80°W. Contours are every 60 gpm.

TABLE 1a. A list of the top 12 analogs. The base date is 0000 UTC 30 January 1966 and the target point is 38°N, 80°W. The unit for rms difference is geopotential meters. The radius of the search area is two grid units (about 900 km).

Year	Month	Day	Hour	Root-mean-square difference
1966	1	30	0	
1970	1	7	12	0.0
1975	1	26	0	47.2
1977	1	25	12	58.1
1971	2	9	12	66.0
1977	1	10	12	67.0
1964	2	8	0	70.9
1969	2	12	0	72.1
1969	1	7	0	78.3
1971	1	26	12	78.4
1967	2	23	12	79.8
1977	2	20	12	80.1
1970	1	8	0	80.9

(see D89 for more discussion on this). From this example it can be seen that certain atmospheric states that are extremely far apart (the rms differences in parentheses in Table 1b) turn into rather similar flows after applying the mirror-imaging operation. In this example, the quality of antilogs and analogs is quite similar. A somewhat undesirable property of antilogs is the clustering of cases in time. The same problem occurs with analogs searched for over large areas (Ruosteenoja 1988). This feature is a drawback when combining two or more cases with the purpose of smoothing the forecast.

We went on to make forecasts, verifying 12 h after the following 20 base dates: 0000 UTC 27 January, 1200 UTC 27 January, . . . 1200 UTC 5 February, for all 15 yr of the dataset. In all, 300 base cases were used, covering a large spectrum of synoptic flows during winter. In each of the 300 cases, we made 10 forecasts (based on the 10 best analogs, excluding neighbors in time), so that the statistics presented here are based on 3000 forecasts. The target point was always at 38°N, 80°W and ana- and antilogs were selected from 0000 UTC 27 December through 1200 UTC 5 March. The 3000 cases were stratified according to their quality; i.e., $0 < Q < 10$, $10 < Q < 20$, etc. We calculated the initial error at the target point over the M cases in each bin as follows:

$$\text{initial error} = \left[\frac{1}{M}\sum_i (B_i - A_i)^2\right]^{1/2}, \qquad (2)$$

and the forecast error was similarly calculated. (Note that M is different for each bin.)

Discussing the AD in this section first, we have plotted frequency distributions of Q for analogs and antilogs in Fig. 2. Averaged over all 3000 cases the initial error is 33.0 and 40.3 gpm for the 10 best analogs and antilogs, respectively. These qualities are about as good as one can hope for given the observational error. The main result is that the two frequency distributions in Fig. 2 are rather similar, but it is worth noting two interesting differences. The first, with antilogs there are fewer excellent matches ($Q < 20$). Second, there are a few flow patterns (only three out of three hundred) for which no passable antilog match can be found (this accounts for all cases where $Q > 110$; remember that 10 antilogs are used for each base case). With regard to the first point the following simple question arises: How to determine the climate [(C) in (1)]? We tried all reasonable estimates of the climate advocated in the literature but found no convincing grounds to prefer one over the other. We settled for the grand mean over 15 yr and all days within the 27 December–5 March window.

Upon investigation of the second point we found that the three base cases for which not even a single passable antilog can be found have the same feature in common, namely, a very deep low in the area considered. While good analogs are available for deep lows there are no antilogs, because as seen in Fig. 3, an extremely deep low turns, upon mirror imaging, into an unrealistic (unobservable) high. A small negative skewness in the height distribution is common equatorward of the jet stream and has qualitatively been explained by White (1980) and Trenberth and Mo (1985). Focusing, however, on the three individual flow patterns (deep lows), the skewness in the height frequency distribution in this area can more specifically be explained from the nonlinearity of the momentum equations. Assuming stationary flow, circular trajectories and a constant Coriollis parameter, the classic gradient wind relation (Holton 1979) implies that for a given radius of the trajectory the pressure gradient has to remain below a critical value in a high, while there is no such limit in a low. Because traveling highs and lows share a common pressure at their boundaries, the asymmetry carries over to pressure (or height) itself.

TABLE 1b. Same as in Table 1a but for antilogs. The values in parentheses are rms differences before mirror imaging.

Year	Month	Day	Hour	Root-mean-square difference
1966	1	30	0	— (0.0)
1974	1	17	0	42.6 (385.0)
1974	1	17	12	52.3 (394.9)
1976	2	14	12	56.1 (351.5)
1974	1	16	12	58.4 (367.5)
1974	1	16	0	66.9 (342.5)
1971	2	18	12	74.3 (329.9)
1968	1	20	0	75.6 (367.9)
1975	2	2	0	76.4 (351.8)
1975	2	1	0	79.2 (363.0)
1968	1	21	12	81.7 (344.7)
1975	1	31	12	82.7 (341.4)
1975	2	1	12	83.3 (353.3)

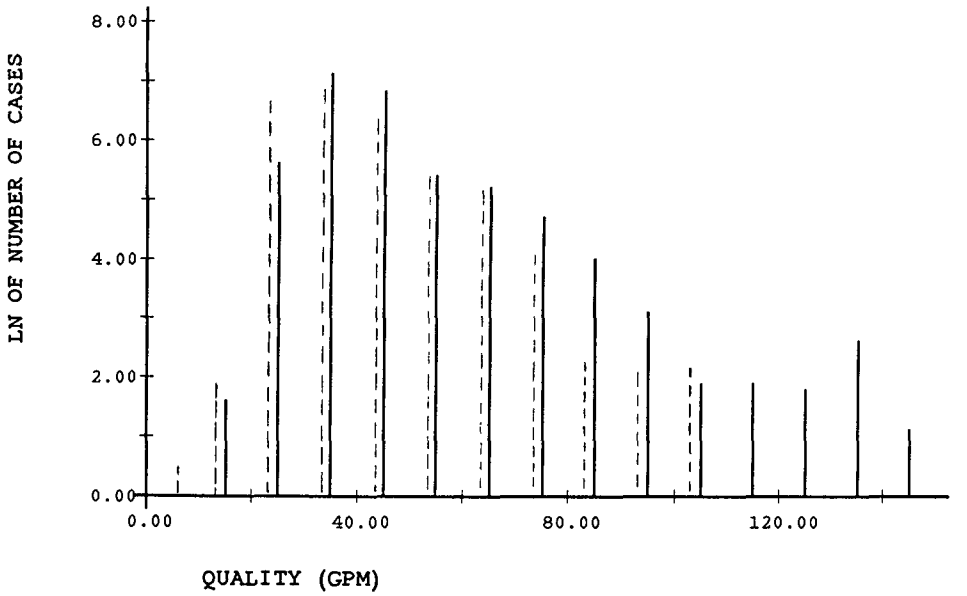

FIG. 2. Frequency distribution of the quality of 3000 analogs (dashed bars) and antilogs (full bars). Along the vertical axis is plotted the natural logarithm of frequency of occurrence [i.e., with reference to Eq. (2) $\ln(M)$].

In this simple explanation nonlinearity of the dynamics carries qualitatively over to an asymmetry of the statistical frequency distribution of pressure and height such that rare large negative departures balance more common smaller positive anomalies; i.e. negative skewness.

c. 12-h height forecasts based on analogs and antilogs

The results of the 3000 analog forecasts for 38°N, 80°W are summarized in Table 2. Over the 300 base cases the analogs 1 through 10, verified individually, feature an initial error of 33.0 and a 12-h forecast rms error of 72.6 gpm. The antilogs have slightly larger initial (40.3) and forecast error (76.8). Both analogs and antilogs outperform persistence although not by much. As shown in D89 the analog forecasts improve drastically upon combining the five best analogs in a weighted manner. The results of the weighted analogs and antilogs ("anaw, antiw") are shown in lines (4) and (5) of Table 2. It is seen then that to first-order approximation the behavior of analogs and antilogs is rather similar. This is empirical evidence that mirror images of atmospheric flow feature mirror-imaged subsequent time tendencies. One wonders whether the antilog forecasts are a bit worse only because the initial match is poorer. In order to place analogs and antilogs on equal footing in a forecasting contest we also considered analogs 11–20 and 21–30, which feature an initial error (averaged over 3000 cases) of 40.2 and 44.6, respectively. Comparing lines (2) and (6) one can see that individual antilogs and analogs have very similar forecast errors when the initial error is similar. However, upon weighting the first five, the analogs 11–15 appear better than antilogs 1–5. It seems, therefore, that antilogs perform slightly worse in forecasting.

Conclusions, therefore, are (i) first-order mirror-imaged flows are followed by mirror-imaged tendencies, (ii) analogs feature somewhat better forecasts than antilogs not only because the initial match is better but also because the weighted combination of five individual forecasts is more effective in smoothing the forecast. Some support for conclusion (i) can be found for the rather special case of so-called persistent anomalies in Dole and Gordon (1986) and Dole (1989).

TABLE 2. Verification statistics (root-mean-square differences) of 3000 (or 300) 12-h 500-mb height forecasts, verifying at 38°N, 80°W. $B - A$ is the initial discrepancy, $F - V$ the 12-h forecast error, and $F - C$ the forecast amplitude. Lines (1), (2), (6) and (7) refer to individual ana- and antilogs. Lines (4), (5), (8) and (9) to ana- or antilog combined into one forecast by Eq. (4).

	$(B - A)$	$(F - V)$	$(F - C)$	Number of cases
(1) Analog 1–10	33.0	72.6	165	3000
(2) Antilog 1–10	40.3	76.8	155	3000
(3) Persistence	NA	80.3	172	300
(4) Anaw 1–5	19.1	51.6	161	300
(5) Antiw 1–5	30.3	60.3	150	300
(6) Analog 11–20	40.2	79.2	163	3000
(7) Analog 21–30	44.6	81.6	160	3000
(8) Anaw 11–15	25.4	57.3	157	300
(9) Anaw 21–25	28.6	59.6	151	300

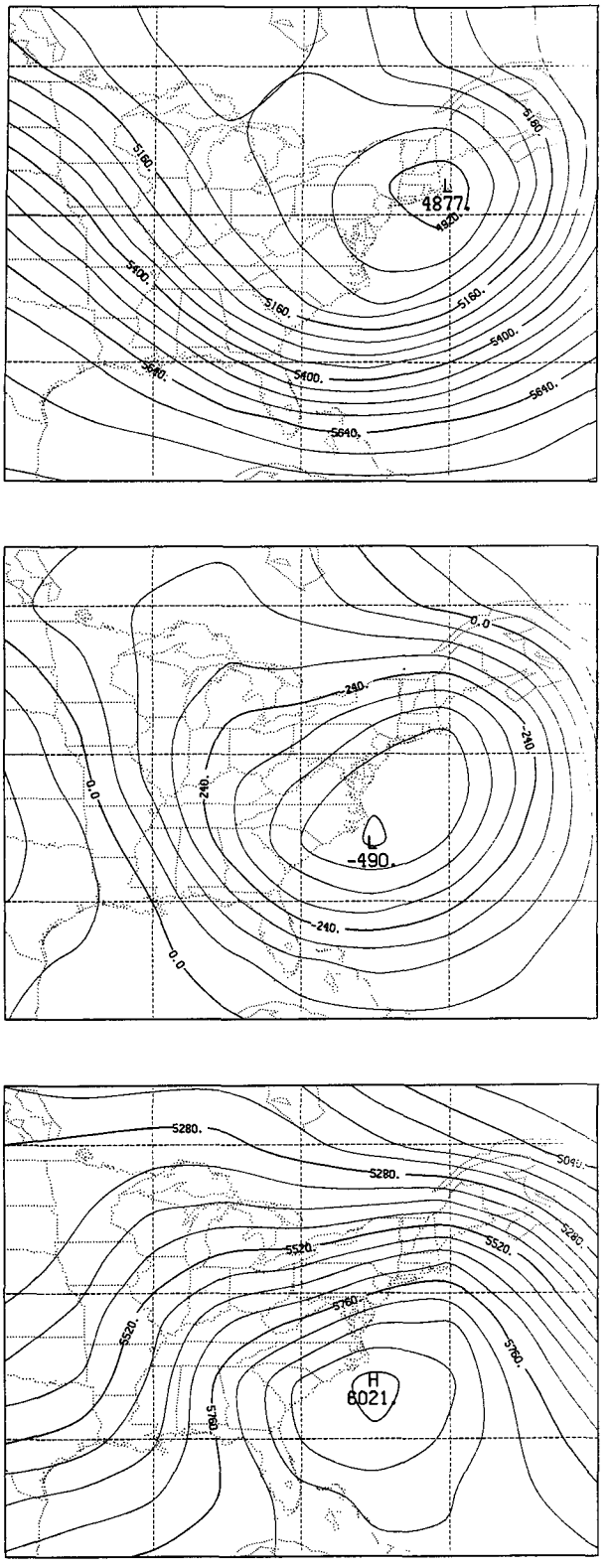

FIG. 3. The 500-mb height map observed at 1200 UTC 27 December 1971 (upper), its departure from climatology (middle), and its mirror image (lower). Contours every 60 gpm.

3. A dynamical hypothesis and test

Assuming divergence to be small, as it is at 500 mb, introducing $x = X_n + x'$ for all variables, where the index n refers to the climate mean and the prime to the anomaly, the anomaly tendency in ζ due to advection can be written as

$$\frac{\partial \zeta'}{\partial t} = -U_n \frac{\partial \zeta'}{\partial x} - u' \frac{\partial \zeta_n}{\partial x} - u' \frac{\partial \zeta'}{\partial x} - V_n \frac{\partial \zeta'}{\partial y} - v' \frac{\partial \zeta_n}{\partial y} - v' \frac{\partial \zeta'}{\partial y} - v' \frac{\partial f}{\partial y} \quad (3)$$

where u and v are the wind components in the zonal (x) and meridional (y) directions. From (3) it is obvious that if one changes the sign of the ζ anomaly on the rhs (which happens if a mirror-imaged height field is used), the tendency of ζ' will change sign too, except when the explicit nonlinearity (i.e., $u'\partial\zeta'/\partial x$ etc.) is large. All other terms can be mirror imaged trivially, even the beta effect. Within the framework of (3) it can thus be stated that antilogs are almost as good as analogs for 12-h forecasts of vorticity or height as long as the nonlinear term is not dominant in producing the anomaly tendency. Below we discuss numerical forecasts to test this idea.

Other than the nonlinear terms in (3) there are several other candidates to break the symmetry between time tendencies following opposite flows. The diabatic heating is an obvious candidate to cause asymmetry in time tendencies. Also the nonlinearity in the divergence term $(f + \zeta)D$ has been mentioned (Dole and Gordon 1983) as a symmetry breaker. Writing the vorticity equation in flux form one can see how this nonlinearity merges with the one in (3).

In the experiments below we employ a model based on the following simplified vorticity equation:

$$\frac{\partial \zeta}{\partial t} = -u \frac{\partial \zeta}{\partial x} - v \frac{\partial \zeta}{\partial y} - \beta v - k\zeta - \nu\nabla^4\zeta + \mathrm{Fo} \quad (4)$$

where Fo is a fixed time-independent forcing, and the dissipation is represented by a linear drag and a fourth-order diffusion. For k we chose 2.5×10^{-6} s^{-1}, and ν is such that at total wavenumber $n = 30$, the linear drag, and diffusion are equal in magnitude. Here, Fo is calculated from

$$\mathrm{Fo} = U_n \frac{\partial \zeta_n}{\partial x} + V_n \frac{\partial \zeta_n}{\partial y} + V_n \frac{\partial f}{\partial y} + k\zeta_n + \nu\nabla^4\zeta_n. \quad (5)$$

On the basis of (4) and (5) a global model was formulated with triangular truncation at zonal wavenumber 30 (T30). Before calculating Fo in (5) the climatological input fields (U_n, V_n) were filtered with a squared exponential filter (Hoskins and Sardeshmukh 1987) that reduces the amplitudes at $n = 27$ to 0.1. The resulting Fo field was further truncated to be within

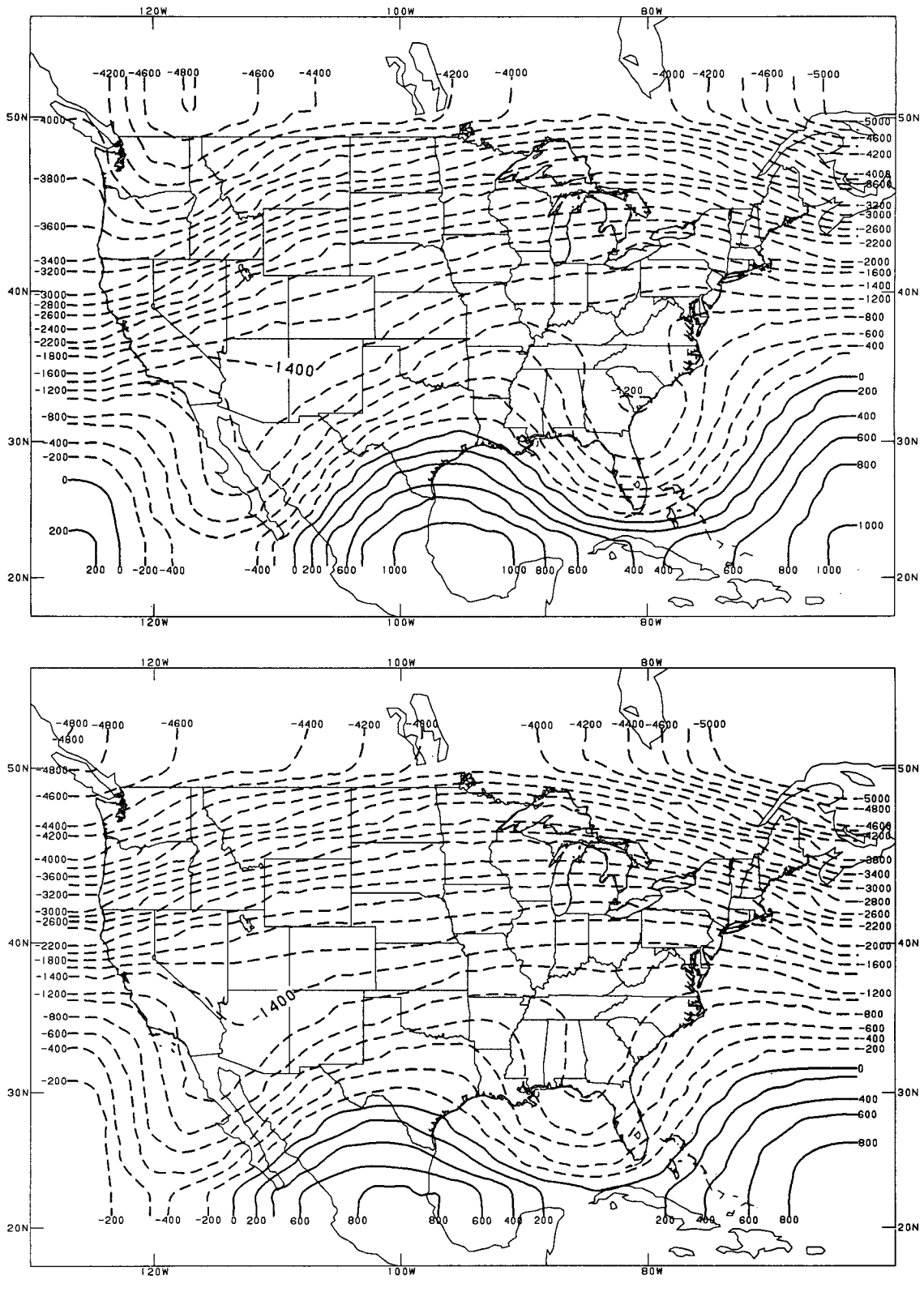

FIG. 4. The streamfunction at 500 mb over the United States at 1200 UTC 22 January 1989 (bottom) and 0000 UTC 23 January 1989 (top). Contour interval $200 \times 10^{+4}$ m^2 s^{-1}.

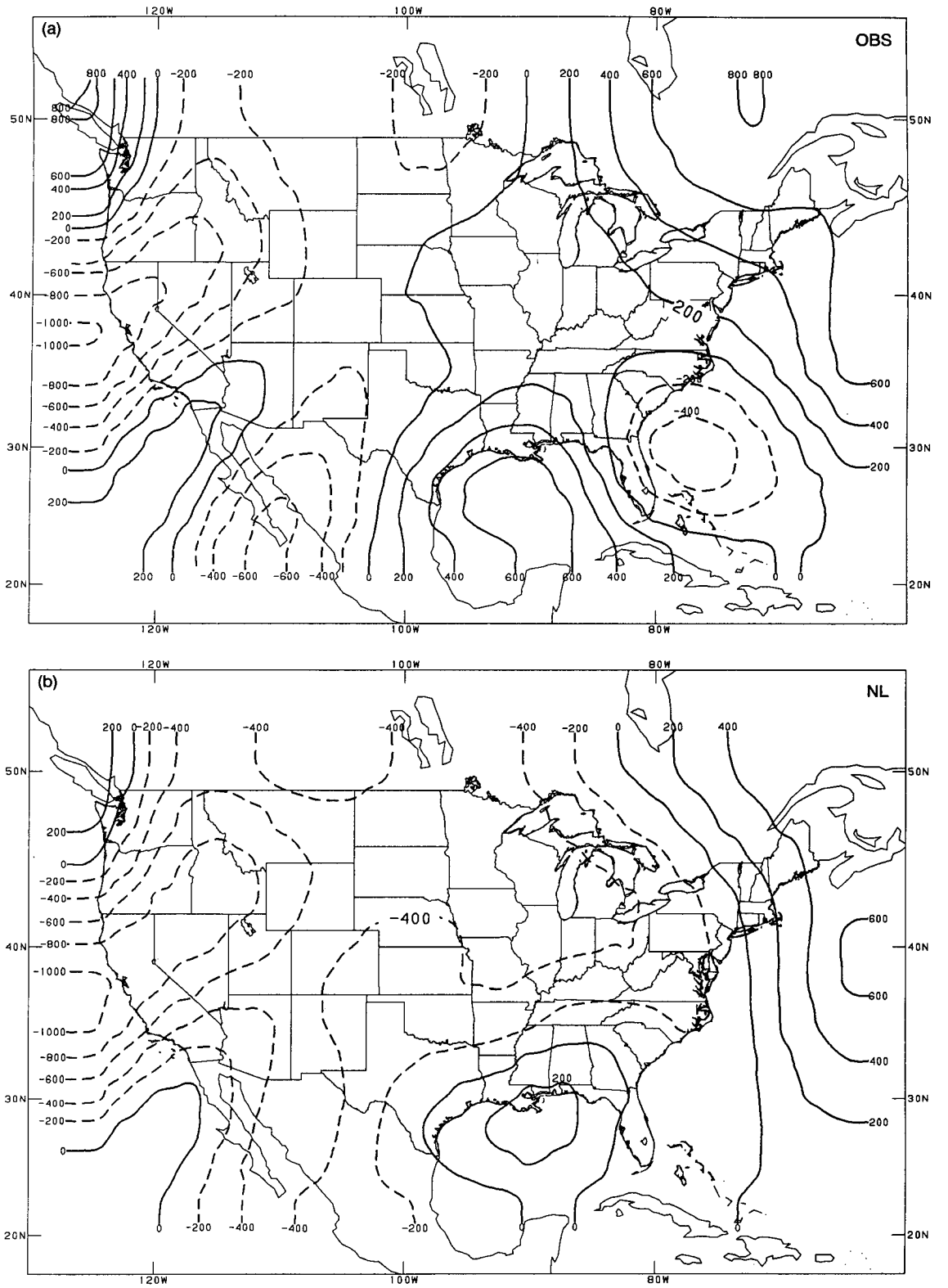

FIG. 5. The difference between the streamfunction at 0000 UTC 23 January 1989 and 1200 UTC 22 January 1989 at 500 mb. Observed 12-h tendencies (a) and by (b) NL, (c) MNL, and (d) L model runs. Contours 200 × 10^{+4} m^2 s^{-1}. The MNL tendency has not yet been mirror imaged.

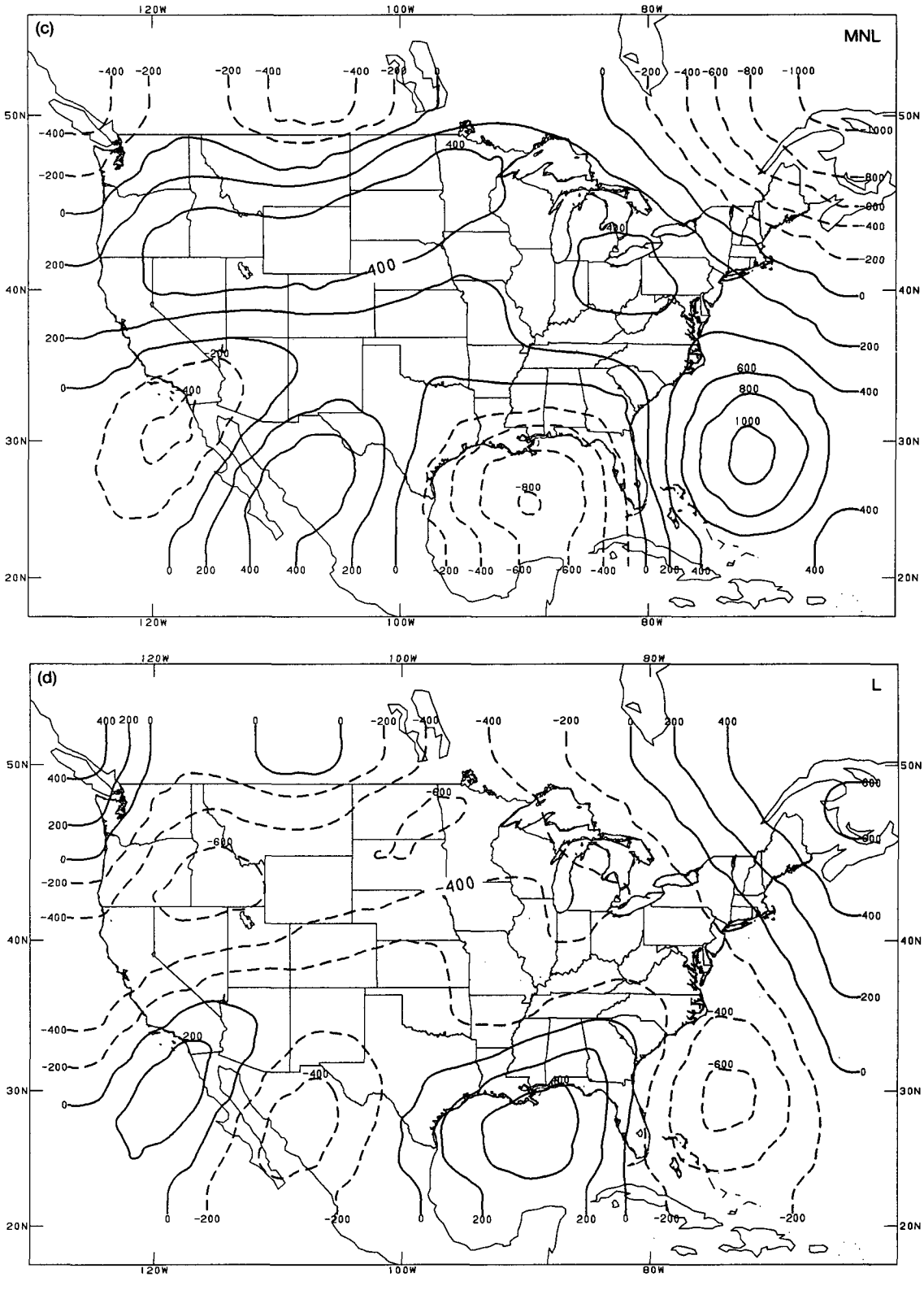

FIG. 5. (*Continued*)

the T30 resolution only. Since we will use January initial conditions to integrate (4) we utilized January climatology (1978–88) in (5). In doing so, (4) essentially describes the time evolution of the anomaly part of ζ, u, and v, even though we solve technically for the full quantities.

Starting from a given observed initial condition (1200 UTC 22 January 1989 for example) we made 12-h forecasts using the three model configurations listed below. In all cases the time step was 1 h, and the model level is 500 mb.

1) *The nonlinear run (NL).* At each time step u and v are calculated from ψ by solving

$$\nabla^2\psi = \zeta$$

and

$$u = -\partial\psi/\partial y$$
$$v = \partial\psi/\partial x \qquad (6)$$

where ψ is the streamfunction. In order to be consistent, the forcing in (5) has to be based on nondivergent winds advecting vorticity. On the whole, (4)–(6) qualify as a rather standard barotropic model except that balancing the climatology is not the classical solution to the spurious retrogression of the long waves (Wolff 1958).

2) *The mirror-imaged nonlinear run (MNL).* Exactly as NL but now starting from the mirror images' initial conditions $\zeta^* = -(\zeta - \zeta_n) + \zeta_n$ and similarly for u and v. At the end of the integration the model solution is mirror imaged again for verification purposes.

3) *The linear run (L).* In this case the advection term is linearized; i.e.,

$$u\frac{\partial\zeta}{\partial x} \text{ becomes } \left[U_n\frac{\partial(\zeta_n + \zeta')}{\partial x} + u'\frac{\partial\zeta_n}{\partial x}\right] \text{ etc.}$$

The forcing in L is the same as in NL and MNL. Although the word linear is appropriate, we point out that the L still has plenty of scale–scale interaction.

If the nonlinear term were zero NL, MNL, and L would give identical forecasts. If the nonlinear process is important we expect the best forecasts to be made by NL, while L should outperform MNL. The NL and MNL solutions are expected to be more different from each other than from the L solution.

We made several integrations but show only those from the initial conditions at 1200 UTC 22 January 1989. These initial conditions were obtained from NMC's global data assimilation system. In Fig. 4 we show for the United States area, the initial streamfunction at 1200 UTC 22 January and the verifying streamfunction 12 h later. The 12-h tendencies produced by NL, MNL, and L, and as they were actually observed are shown in Fig. 5. The level of agreement in forecast ψ tendencies between the three methods is quite remarkable. The results from the numerical integration thus lend some support to the empirical finding that analogs and antilogs make for 12-h height forecasts of rather comparable skill. (Comparing the results of the barotropic model and empirical AF is valid only in midlatitudes where height and streamfunction have a very similar spatial scale.)

Forecasts were also studied in terms of the smaller-scale vorticity fields (not shown). Here the expected order, NL the best, MNL the worst, and L in between, stands out very clearly. In the smaller scales the correct representation of the nonlinearity is important in far less than 12 h for perturbations as large as day-to-day anomalies.

4. Conclusions and discussion

We earlier made a set of 3000 12-h 500-mb height forecasts using the limited-area analogs approach as described in D89. This experiment has now been supplemented by 3000 antilog forecasts. A pair of antilogs are two flow patterns that, relative to climatology, are each other's opposite as much as possible. A forecast is obtained by mirror imaging the flow that follows the historical antilog. The comparison of analogs and antilogs and the forecasts based on them over eastern North America yields the following conclusions:

1) For almost all flow patterns it is almost as easy to find an antilog as an analog. Exceptions are very deep lows for which no mirror-imaged highs exist.

2) Antilogs make for 12-h forecasts at a skill level almost as good as those based on analogs.

The first conclusion indicates that flow patterns are rather symmetric relative to climatology, a diagnostic result in agreement with but expanding on White (1980) and Trenberth and Mo (1985) who investigated, point by point, the skewness of height distributions. Therefore, mirror imaging an observed flow is likely to yield a physically plausible pattern although not necessarily one observed so far. Of interest now is the more general question, Is it possible to construct plausible patterns from observed flows? Not just by mirror imaging, but by any linear combinations of past flows?

The lack of symmetry for some flows (the deep lows) can perhaps be explained by the nonlinearity of the momentum equations that allow a larger pressure gradient in lows than in highs. In this sense asymmetry and nonlinearity are related.

The second conclusion deals with a prognostic aspect, namely that time tendencies tend to be opposite for opposite initial conditions. This kind of symmetry is perhaps unexpected because for large perturbations

linearity is not a good assumption. Indeed the idea of antilogs was never before applied to instantaneous flow. An explanation for the quasi-linear behavior over short times is sought by running a global barotropic model from both regular and mirror-imaged conditions. We found

3) Out to 12 h the tendency of the midlatitude streamfunction is primarily determined by the linear part of the absolute vorticity advection. The explicit nonlinearity is made as small as possible by decomposing vorticity and wind in a constant climatological mean plus a variable anomaly.

4) A barotropic model linearized with respect to the climate is, therefore, almost as good as a regular nonlinear barotropic model for short-term forecasts of height.

5) However, the vorticity forecasts deteriorate after only 6 h when the nonlinear term is either omitted or represented incorrectly (in the mirror-imaged run).

Conclusion 3 would be an explanation of the empirical prognostic findings concerning analogs and antilogs; except that we don't know for a fact that analogs behave like a barotropic model. We speculate, however, that this is the case because if two atmospheric states have the 500-mb height field in common in some area, then the vorticity advection ought to be the same. Conclusion 4 appears to be in agreement with the success of Roads' (1990) linear time-dependent model. While we have not produced proof that AF works like a barotropic model, we have not found inconsistencies that would suggest otherwise.

We must emphasize once more that no quantitative statement about nonlinearity can be made without reference to a basic state. By using the climatology as a basic state we have made the explicit nonlinearity among the anomalies rather small, probably close to the absolute minimum.

Because the definition of antilog invokes the notion of climate it is appropriate to discuss how well we know the climate. In the present study the problem of determining the correct climate appeared mostly to be a practical matter; i.e. how many years and how many harmonics to produce a smooth curve (see Trenberth and Mo 1985 and references), etc. From the Q statistics in Table 2, we infer that we do not have the far more serious problem of a bimodal height distribution. Under those conditions the mean height would no longer represent the climate, and antilogs would be almost impossible to define.

Although we have explained perhaps why analogs and antilogs yield rather similar 12-h forecasts, the fact remains that not much use can be expected from antilogs for forecasting instantaneous flow beyond 12 h. Interestingly the original idea of antilogs was launched in the context of long-range forecasting (Harnack et al. 1985) where a certain utility was claimed. In those studies (Livezey and Barnston 1988; Barnston and Livezey 1989) the task is to find a match to time-mean sea surface temperature, the Southern Oscillation index, and height and thickness fields etc. As shown in van den Dool (1987) and Barnston and Livezey (1989) including antilogs apparently improves the monthly and seasonal forecast, although the reasons are not quite clear. For instantaneous flow (this paper) the success of antilogs in forecasting depends on the importance of the linear part of advection in creating tendencies. For time-mean flow tendencies are negligible and one must, for example, assume that somehow the time evolution of the external forcing anomalies (as well as attendant atmospheric response) is opposite for mirror-imaged initial time-mean conditions. The diagnostic component, the existence of anomaly fields that are each other's opposite, is well established for time-mean fields of many parameters; in fact more convincingly so than for instantaneous flows. For instance teleconnectivity maps (Wallace and Gutzler 1981) and the specification of surface weather from upper level charts (Klein and Bloom 1987) all make a tacit assumption of linearity by using linear correlations. But a sound physical basis to explain the "linearity" of time-mean fields as well as the (modest, if any at all) success of antilog forecasting in the long range has yet to be given.

Acknowledgments. The author thanks the following colleagues for their helpful comments: R. E. Livezey, J. R. Lanzante, M. Cai, J. O. Roads, Z. Toth, Jeff Anderson, and A. G. Barnston. The research was supported by NOAA under Grant NA89-AA-H-MC066.

REFERENCES

Barnston, A. G., and R. L. Livezey, 1989: An operational multifield analog/anti-analog prediction system for United States seasonal temperatures. Part II: Spring, summer, fall and intermediate 3-month period experiments. *J. Climate,* **2,** 513–541.

Dole, R. M., 1989: Life cycles of persistent anomalies. Part I: Evolution of 500 mb height fields. *Mon. Wea. Rev.,* **117,** 177–211.

——, and N. D. Gordon, 1983: Persistent anomalies of the extratropical Northern Hemisphere wintertime circulation: geographical distribution and regional persistence characteristics. *Mon. Wea. Rev.,* **111,** 1567–1586.

Gutzler, D. S., and J. Shukla, 1984: Analogs in the wintertime 500 mb height field. *J. Atmos. Sci.,* **41,** 177–189.

Harnack, R., M. Cammarata, K. Dixon, J. Lanzante and J. Harnack, 1985: Summary of United States seasonal temperature forecast experiments. *Proc. of the Ninth Conf. on Probability and Statistics in Atmospheric Sciences.* Virginia Beach, 175–179.

Holton, J. R., 1979: *An Introduction to Dynamic Meteorology.* Academic Press, 391 pp.

Hoskins, B. J., and P. D. Sardeshmukh, 1987: Transient eddies and the seasonal mean rotational flow. *J. Atmos. Sci.,* **44,** 328–338.

Klein, W. H., and H. J. Bloom, 1987: Specification of monthly precipitation over the United States from surrounding 700 mb height fields in winter. *Mon. Wea. Rev.,* **115,** 2118–2132.

Livezey, R. E., and A. G. Barnston, 1988: An operational multifield analog/anti-analog prediction system for United States seasonal temperatures. Part I: System design and winter experiments. *J. Geophys. Res.*, **93,** 10 953–10 974.

Lorenz, E. N., 1969: Atmospheric predictability as revealed by naturally occurring analogs. *J. Atmos. Sci.*, **26,** 636–646.

Roads, J. O., 1990: Linear model predictions of time averages. *J. Climate,* **3,** 317–336.

Ruosteenoja, K., 1988: Factors affecting the occurrence and lifetime of 500 mb height analogs: A study based on a large amount of data. *Mon. Wea. Rev.*, **116,** 368–376.

Shabbar, A., and J. L. Knox, 1986: Monthly prediction by the analog method. *Proc. of the First WMO Workshop on the Diagnosis and Prediction of Monthly and Seasonal Atmospheric Variations Over the Globe,* Geneva, World Meteorological Organization, 672–681.

Toth, Z., 1991: Intercomparison of circulation similarity measures. *Mon. Wea. Rev.*, **119,** 55–64.

Trenberth, K. E., and K. C. Mo, 1985: Blocking in the Southern Hemisphere. *Mon. Wea. Rev.*, **113,** 3–21.

van den Dool, H. M., 1987: A bias in skill in forecasts based on analogs and antilogs. *J. Climate Appl. Meteor.*, **26,** 1278–1281.

——, 1989: A new look at weather forecasting trough analogs. *Mon. Wea. Rev.*, **117,** 2230–2247.

Wallace, J. M., and D. S. Gutzler, 1981: Teleconnections in the geopotential height field during the Northern Hemisphere winter. *Mon. Wea. Rev.*, **109,** 784–812.

White, G. H., 1980: Skewness, kurtosis, and extreme values of Northern Hemisphere geopotential heights. *Mon. Wea. Rev.*, **108,** 1446–1455.

Wolff, P., 1958: The error in numerical forecasts due to retrogression of ultra-long waves. *Mon. Wea. Rev.*, **86,** 245–250.